

## Paper:

# Analysis of Autonomous Coordination Between Actuators in the Antagonist Musculoskeletal Model

Takahiro Goto\*, Yasuhiro Sugimoto\*, Daisuke Nakanishi\*\*,  
Keisuke Naniwa\*\*\*, and Koichi Osuka\*

\*Osaka University

2-1 Yamadaoka, Suita, Osaka 565-0871, Japan

E-mail: {t.goto@dsc., yas@, osuka@}mech.eng.osaka-u.ac.jp

\*\*National Institute of Technology, Matsue College

14-4 Nishi-ikuma, Matsue, Shimane 690-8518, Japan

E-mail: nakanishi@matsue-ct.jp

\*\*\*Hokkaido University

Kita 12, Nishi 7, Kita-ku, Sapporo, Hokkaido 060-0812, Japan

E-mail: naniwa@es.hokudai.ac.jp

[Received March 10, 2020; accepted February 24, 2021]

The McKibben Pneumatic Actuator (MPA) is well-known as a type of soft actuator. As MPA generates tension only in the direction of compression, it is necessary to construct an antagonistic structure to drive a joint by MPAs and to coordinate antagonized MPAs. Similar to MPA, muscles in animals also generate tension only in the direction of contraction. Some studies have reported that animals utilize tension information to coordinate muscles for various autonomous movements. The purpose of this study is to realize autonomous cooperation between antagonized MPAs by applying tension feedback control and analyzing the mechanism of coordination. For this purpose, we verify the effect of tension feedback control on the 1-DOF pendulum model with antagonized MPAs. First, through numerical simulations, it is confirmed that the tension feedback generates various coordinated movements of antagonized MPAs, and the pendulum exhibits a bifurcation phenomenon based on the phase difference of the inputs of MPAs. Thereafter, we develop an actual experimental machine based on the model and confirm the autonomous cooperation between actual MPAs through verification experiments similar to the numerical simulations.

**Keywords:** pneumatic artificial muscle, actuator cooperation, tension feedback, antagonistic structure

## 1. Introduction

The McKibben Pneumatic Actuator (MPA) is a type of soft actuator that is driven by air pressure. As shown in Fig. 1, MPA consists of a silicone rubber tube covered with a nylon mesh. By applying air pressure, the actuator contracts along the direction of the long axis. It is



Fig. 1. Overview of MPA at normal state (bottom) and contraction state (top).

often utilized in rehabilitation devices because of its flexibility and high back drivability [1]. Furthermore, the MPA is also utilized in robots that imitate animals owing to its high output per mass, and the robot achieves jumping motion with its simple input [2]. However, due to the complexity of the MPA model, the input design of each MPA to drive a robot is often done by trial-and-error parameter tuning. And there has been little theoretical analysis of MPA coordination and the resulting robot motion. Therefore, this study aims to achieve autonomous robot movements by controlling the coordination between MPAs. Autonomous motion generation leads to various motions without relying on parameter tuning.

As the MPA generates tension only in the direction of compression, it is necessary to construct an antagonistic structure to drive a joint by MPAs. Similar to MPA, muscles generate tension only in the direction of contraction. For this reason, multiple muscles are located on one joint in animals. Motion is generated by the appropriate tension and relaxation of muscles involved in the movement of each joint. Therefore, MPA-driven robots must achieve

proper coordination between MPAs.

Various coordination skills are involved in the movements of animals. For example, animals can walk without falling over even on uneven terrain by skillfully moving their legs according to the surrounding terrain. The realization of such adaptive gait is fascinating, and various studies have been conducted to elucidate the mechanism. Experiments with animals suggest that the gait of animals is not always controlled by the brain; instead, the gait rhythm emerges at the spinal cord due to a neural circuit called the central pattern generator (CPG) [3]. Animals use this CPG to achieve periodic movements of flexor and extensor muscles. It has also been reported that sensory information is used for gait control in addition to the CPG [4]. These findings suggest that animals achieve coordination based on the feedback of sensory information obtained from interactions with the surrounding environment in addition to the rhythm generated by CPG.

Several studies have already attempted to model the movement of animals realized by coordination. For example, several CPG models expressed as neural oscillator systems have been proposed for walking. Some models can realize the robust bipedal walking or quadrupedal walking with feedback of sensory information [5, 6]. A few studies have focused on the interaction between the body and the surrounding environment during walking. Ishiguro et al. proposed the “TEGOTAE” control method, which uses force information obtained from the surroundings [7]. Although this control method does not include direct coordination between the legs, it can produce coordination between the legs through interaction with the environment and acknowledge an adaptive gait according to the walking speed, etc.

On the contrary, the cooperative relationships for an adaptive gait exist not only in inter-leg coordination but also in intra-leg coordination. It has been revealed that animals walk stably by flexibly changing the contraction timing of the muscles in their legs in response to changes in the environment [8, 9]. Therefore, it is noteworthy that the cooperative relationship between muscles in the antagonistic structure is also an essential factor for the realization of autonomous movement.

Considering the above-mentioned description, in this study, we attempt to realize an autonomous, cooperative relationship of antagonized MPAs with the musculoskeletal robot model and investigate the mechanism of the resultant coordination of MPAs. To realize the coordination between antagonistic actuators, we focus on the fact that animals use sensory information such as muscle length and tension during walking [4]. For this purpose, in this study, we first construct a new tension feedback control law. Through numerical simulations, we confirm that the tension feedback generates various coordinations of antagonized MPAs, and the pendulum exhibits a bifurcation phenomenon based on the phase difference of the inputs of MPAs. Subsequently, we develop an experimental system based on the model and confirm autonomous cooperation between actual MPAs through verification experiments similar to the numerical simulations. These results

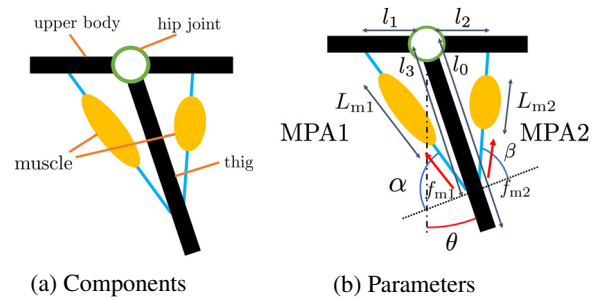


**Fig. 2.** Model of the 1-DOF pendulum driven by antagonistic actuator.

**Table 1.** Parameters of 1-DOF pendulum.

Symbols	Definitions	Values
$l_0$	Pendulum length	550 mm
$\theta_0$	Initial pendulum angle	0 rad
$m$	Pendulum mass	1 kg
$g$	Gravitational acceleration	9.80665 m/s <sup>2</sup>
$l_1, l_2$	Offset between the rotation center and the upper attachment position of MPA	30 mm
$l_3$	Length to MPA attachment position in rod pendulum	500 mm
$L_0$	Natural length of MPA	300 mm
$D_0$	Natural diameter of MPA	15 mm
$l_{w1}, l_{w2}$	Wire length of MPA	200.9 mm

suggest that the tension feedback control realizes the various movement of multi-joint robots with MPAs by controlling the coordination between MPAs.

## 2. Leg Model and Control Law

### 2.1. Model of Monarticular Leg Driven by Antagonist Muscles

For the theoretical analysis, our study focused on a one-leg model with a simple antagonistic structure. **Fig. 2(a)** presents the model to be analyzed. This model consists of the upper body, thigh, hip joint, and two antagonized MPAs. This model can be considered as a 1-DOF symmetric pendulum. As shown in **Fig. 2(a)**, the component supporting the pendulum corresponds to the upper body, the center of rotation of the pendulum corresponds to the hip joint, and the pendulum corresponds to the leg. Moreover, the antagonized MPAs drive the pendulum.

**Figure 2(b)** shows parameters of the rod pendulum model. The details of each parameter in **Fig. 2(b)** are shown in **Table 1**. It is assumed that the rod pendulum has a constant density and that the vertically downward direction is 0 rad.

The equation of angular motion around the joint can be derived as follows:

$$I\ddot{\theta} = f_{m1}l_3 \cos \alpha - f_{m2}l_3 \cos \beta - \frac{1}{2}mgl_0 \sin \theta, \quad (1)$$

where  $I$  is the moment of inertia,  $\alpha$  and  $\beta$  are the angles formed by the pendulum and the tension direction of MPA1 and MPA2, respectively.  $\alpha$  and  $\beta$  are calculated as follows:

$$\cos \alpha = \frac{l_1 \cos \theta}{L_{m1} + l_{w1}}, \cos \beta = \frac{l_2 \cos \theta}{L_{m2} + l_{w2}}. \dots (2)$$

Each MPA length is determined by the pendulum angle  $\theta$  according to the geometric relationship as follows:

$$\begin{cases} L_{m1} = \sqrt{l_1^2 + l_3^2 - 2l_1l_3 \sin \theta} - l_{w1}, \\ L_{m2} = \sqrt{l_2^2 + l_3^2 - 2l_2l_3 \sin \theta} - l_{w2}. \end{cases} \dots (3)$$

The MPA contraction velocities  $v_i = \dot{L}_{mi}$  ( $i = 1, 2$ ) are obtained from the pendulum velocity as follows:

$$\begin{cases} v_1 = \frac{l_1 l_3 \cos \theta}{\sqrt{l_1^2 + l_3^2 - 2l_1l_3 \sin \theta}} \dot{\theta}, \\ v_2 = -\frac{l_2 l_3 \cos \theta}{\sqrt{l_2^2 + l_3^2 + 2l_2l_3 \sin \theta}} \dot{\theta}. \end{cases} \dots (4)$$

### 2.2. Tension Model of MPA

Several studies have proposed tension models for MPA [10, 11]. In this study, we use the linear approximation model, which was proposed in our previous study, to analyze the effect of MPA characteristics on movement [12]. It has been confirmed that this model can appropriately express the tension characteristics of MPA despite its simplistic form, as compared to other proposed models. The linear approximation model is expressed as follows:

$$f_m(P', L_m, v) = S_1 P' + S_2 P' L_m + S_3 L_m + S_4 + \gamma v \quad (5)$$

where  $S_{1,2,3,4}$  and  $\gamma$  are constant. The MPA tension is calculated by substituting the MPA pressure  $P'$ , length  $L_m$ , and contraction velocity  $v$  into The details of this tension model of MPA are provided in Appendix A.

### 2.3. Tension Feedback Control Method

To develop a tension feedback control method applicable for the MPAs, the ‘‘TEGOTAE’’ control law [7] is referred. The ‘‘TEGOTAE’’ control law is a phase oscillator-based control method that uses sensory information of the ground reaction force of each leg for modifying the intrinsic angular velocity of the oscillator, to reproduce the cooperative movement between legs. An important feature of the ‘‘TEGOTAE’’ control law is its ability to produce autonomous coordination between the legs without implementing direct inter-leg coordination. In this study, using tension feedback control, we realize autonomous coordination between MPAs and realize various pendulum motions.

The tension feedback control law for MPAs used in this study is defined as follows:

$$\dot{\phi}_i = \omega - \sigma f_{mi} \cos \theta \quad \dots (6)$$

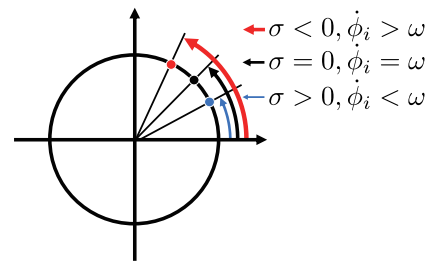


**Fig. 3.** Effect of tension feedback to phase oscillator. The angular velocity of oscillator is greater than the intrinsic angular velocity  $\omega$  with negative feedback gain  $\sigma$ , and the angular velocity is slower with positive feedback gain  $\sigma$ .

where  $\phi_i$  is the phase of oscillator assigned to each MPA,  $f_{mi}$  ( $i = 1, 2$ ) is the tension of the MPAs, which corresponds to the sensory information obtained in the model,  $\theta$  is the pendulum angle representing the state of the pendulum,  $\omega$  is the intrinsic angular velocity, and  $\sigma$  is the feedback gain. The second term expresses the tension feedback. This term modifies the periodic motion with the intrinsic angular velocity if there is tension of the MPAs. Furthermore, the angular velocity of the phase oscillator is modified depending on the feedback gain sign, as shown in **Fig. 3**. When there is a significant swing of the pendulum, the effect of feedback is reduced because the tension feedback is directly proportional to  $\cos \theta$ . The tension feedback term results in a difference in the angular velocity of the two-phase oscillators. This difference causes a change in the relationship between the antagonistic actuators.

The MPA expands and contracts when a pressure input is applied. In this study, the input pressure  $P'_i$  ( $i = 1, 2$ ) to MPA1 and MPA2 are defined by substituting  $\phi_i$  in Eq. (6) into the following equation:

$$P'_i = A(1 - \sin \phi_i) \quad \dots (7)$$

where  $A$  is the pressure amplitude. One rotation of the phase oscillator on the circle is equivalent to the MPA performing contraction and extension once. Hence, the pendulum swings one cycle.

Here, the phase difference is defined as follows:

$$\phi = \phi_1 - \phi_2. \quad \dots (8)$$

## 3. Simulation of a 1-DOF Pendulum

We simulated the motion of the pendulum model and tension feedback described in Section 2 and thus verified that a cooperative relationship could be created and determined the type of cooperative relationship that could be created.

### 3.1. Realization of Autonomous Cooperation Between Actuators

This section describes an example of the motion realized by the proposed tension control law and the ability to

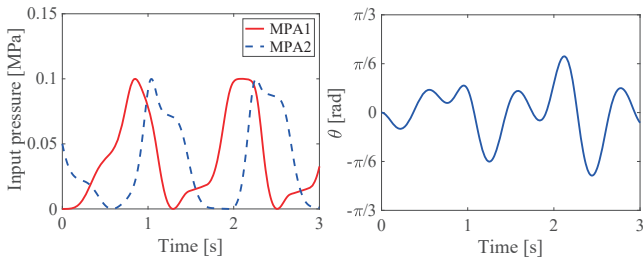


**Fig. 4.** Simulation result of 1-DOF pendulum with  $\omega = 0.20\pi$  rad/s and  $\sigma = -0.075$  ( $t = 0-3$  s).

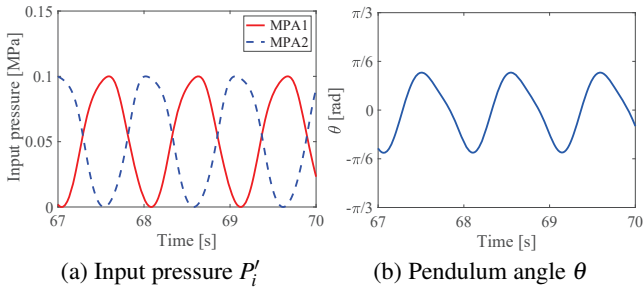


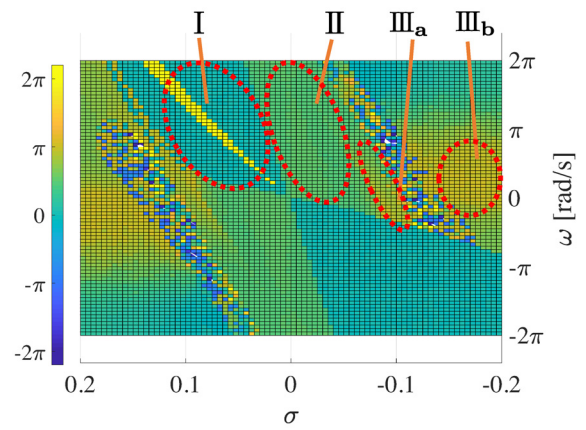
**Fig. 5.** Simulation result of 1-DOF pendulum with  $\omega = 0.20\pi$  rad/s and  $\sigma = -0.075$  ( $t = 67-70$  s).

generate an autonomous cooperative relationship.

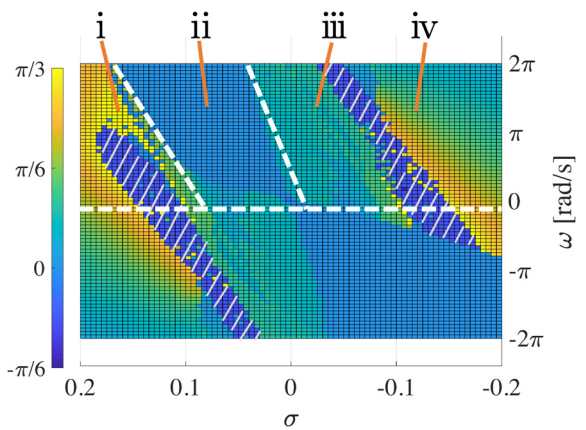
**Figure 4** presents the simulation results for 0–3 s with  $\omega = 0.20\pi$  rad/s,  $\sigma = -0.075$  and the initial phase difference  $\phi_0 = \pi/2$  rad. **Fig. 4(a)** shows the input pressures of MPAs against time, and **Fig. 4(b)** shows the pendulum angle against time. The pendulum motion is irregular due to the initial phase difference, as shown in **Fig. 4(b)**. **Fig. 5** shows the simulation results while 67–70 s under the same conditions. As shown in **Fig. 5(a)**, the pressures of MPAs became periodic and a roughly anti-phase wave. In addition, the motion of pendulum also became periodic in **Fig. 5(b)**. In this case, the phase difference  $\phi$  transitioned from the initial phase difference  $\pi/2$  rad to near  $\pi$  rad. Comparing **Figs. 4** and **5**, the relationship between the pressure of MPAs transitioned autonomously, and then, the pendulum realized the periodic motion. These results suggest that the tension feedback control can realize autonomous cooperation between the actuators.

### 3.2. Analysis of Relationship Between Intrinsic Angular Velocity and Feedback Gain

Next, the effect of the tension feedback control on the resultant pendulum motion was verified. For this purpose, we conducted simulations while changing the intrinsic angular velocity  $\omega$  rad/s and the feedback gain  $\sigma$  parameters in the tension feedback control law. The parameter range of the simulation was  $-2.00\pi$  rad/s  $\leq \omega \leq 2.00\pi$  rad/s,  $-0.200 \leq \sigma \leq 0.200$ . Furthermore, to obtain a steady-state result, the average phase difference  $\bar{\phi}$  and amplitude while 70–80 s are focused. The average amplitude is defined as an average peak value of the simulation result between 70–80 s.



(a) Average phase difference ( $\sigma$ - $\omega$  plane)



(b) Average amplitude ( $\sigma$ - $\omega$  plane)

**Fig. 6.** The simulation results of tension feedback with initial phase difference  $\pi/2$  rad.

**Figure 6** shows the simulation results for the initial phase difference  $\pi/2$  rad. In the figure, the feedback gain  $\sigma$  is on the  $x$ -axis; the intrinsic angular velocity  $\omega$  of the phase oscillator is on the  $y$ -axis. The average phase difference  $\bar{\phi}$  or amplitude is represented on the  $\sigma$ - $\omega$  plane by the color shown in the color bar.

As shown in **Fig. 6(a)**, the average phase difference  $\bar{\phi}$  or amplitude significantly differs based on parameters. There are also regions with clear boundaries. In the region II, the average phase difference  $\bar{\phi}$  does not change from the initial value  $\pi/2$  rad. This is because the feedback gain is small with respect to the intrinsic angular velocity, and then the tension feedback did not affect it.

In regions other than region II, the average phase difference  $\bar{\phi}$  transitioned from  $\pi/2$  rad to other values depending on the choice of parameters. The region III in **Fig. 6(a)** is the region where the average phase difference  $\bar{\phi}$  transitioned to the neighborhood of  $\pi$ . It should be noted that the regions III<sub>a</sub> and III<sub>b</sub> are not connected. A chaotic region exists between the region III<sub>a</sub> and the region III<sub>b</sub>. As we discuss later, this fact suggests that these regions III<sub>a</sub> and III<sub>b</sub> have different oscillation modes. In addition, the region I is the region where the average phase difference  $\bar{\phi}$  is 0 rad or  $2\pi$  rad.

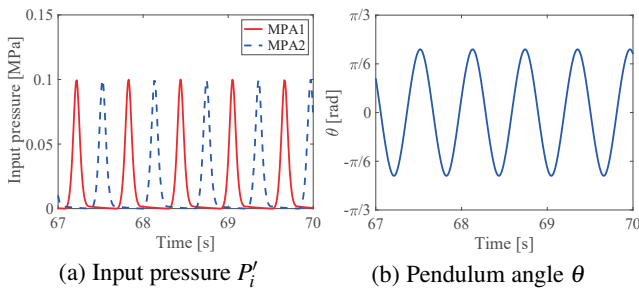


**Fig. 7.** Simulation result of 1-DOF pendulum with  $\omega = 0.20\pi$  rad/s and  $\sigma = -0.170$  ( $t = 67-70$  s).

**Figure 6(b)** shows the average amplitude of pendulum under each parameter. In this figure, when the pendulum angle diverged, the average amplitude was replaced with a negative value (the region between iii and iv). That is, such regions are plotted as hatched areas. Similar to the average phase difference  $\bar{\phi}$ , there are also regions with clear boundaries in this figure. Focusing on the region of  $\omega > 0$  rad/s, it can be seen that the amplitude discontinuously transitions from about  $\pi/3$  rad to 0 rad at the boundary between the regions i and ii as the feedback gain  $\sigma$  decreased. Furthermore, the amplitude discontinuously transitions to the region iii where the amplitude is about  $\pi/6$  rad. As the feedback gain  $\sigma$  further decreased, the region iv where a steady-state is generated again exists beyond the region where the pendulum motion diverges.

Comparing **Fig. 6(a)** with **Fig. 6(b)**, it can be seen that the regions in **Fig. 6(a)** and those in **Fig. 6(b)** correspond well. Especially, the region ii, where the amplitude is 0 rad, matches the region I where the average phase difference  $\bar{\phi}$  is around 0 rad or  $2\pi$  rad well. The regions II and iii also match well. Besides, it can also be seen that the pendulum amplitude tends to be large in the region where the average phase difference  $\bar{\phi}$  is large.

From the above, it was confirmed that the proposed tension feedback generated not only a cooperative relationship, but also various cooperative relationships depending on parameters. Besides, the slight change in the parameters resulted in the mode change of the pendulum motion; e.g., the oscillation mode in the region II changed to stationary mode at 0 rad in the region I. This result suggests that a certain bifurcation phenomenon occurred in the system analyzed in this paper.

### 3.3. Analysis of Characteristic Pendulum Movements

Next, the pendulum motion at the specific points in **Fig. 6** was examined. **Fig. 7** shows the simulation results while 67–70 s with  $\omega = 0.20\pi$  rad and  $\sigma = -0.170$  in the region III<sub>b</sub>. From **Fig. 7(a)**, it can be seen that the input pressures of MPAs also became a rough, anti-phase wave, and the pendulum showed a stable periodic motion in **Fig. 7(b)**. Also with  $\sigma = -0.075$  in the region III<sub>a</sub>, the average phase difference  $\bar{\phi}$  was approximately  $\pi$  rad in **Fig. 6(a)** with  $\sigma = -0.075$ . However, the amplitude in **Fig. 7(b)** is larger than that in **Fig. 5(b)**.

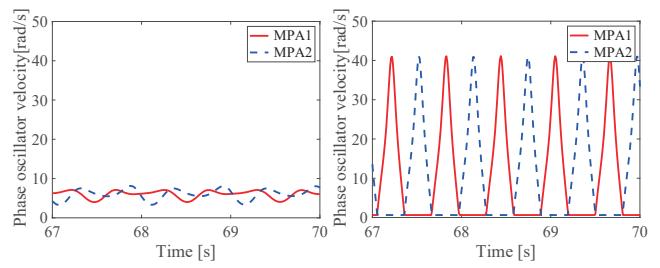


**Fig. 8.** Simulation result of 1-DOF pendulum with  $\omega = 0.20\pi$  rad/s ( $t = 67-70$  s).

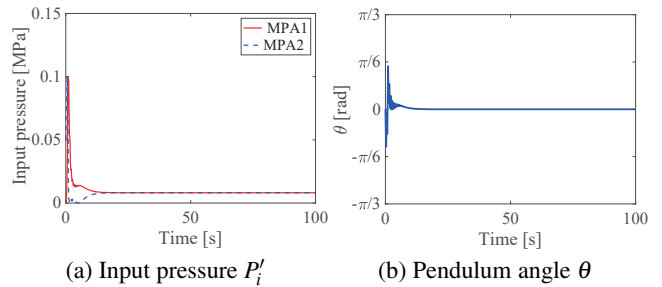


**Fig. 9.** Simulation result of 1-DOF pendulum with  $\omega = 0.20\pi$  rad/s and  $\sigma = 0.050$  ( $t = 0-100$  s).

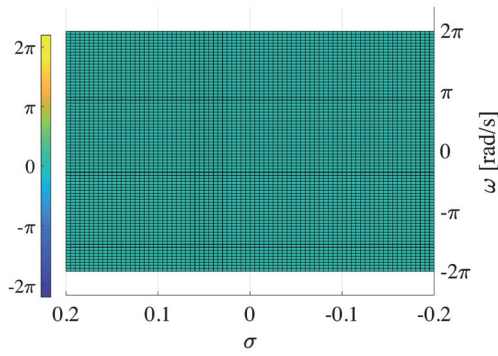
**Fig. 8** shows the angular velocity of the phase oscillators in the case of  $\sigma = -0.075$  or  $\sigma = -0.170$  respectively. From **Fig. 8(a)**, the angular velocity of the two-phase oscillator hardly changes when  $\sigma = -0.075$ . This means that the phase oscillator was moving symmetrically at the origin. In contrast, when one phase oscillator was moving, the other phase oscillator was almost stopped in the case of  $\sigma = -0.170$  (**Fig. 8(b)**). These results indicate that the two oscillators moved alternately. From above, even if the average phase difference  $\bar{\phi}$  looks the same, these two parameters in **Figs. 5** and **7** generated different oscillation modes.

**Figure 9** shows the simulation results while 0–100 s when  $\omega = 0.20\pi$  rad/s and  $\sigma = 0.050$ . From **Figs. 9(a)** and **(b)**, the input pressures of MPAs became non-zero constant, and the pendulum stopped moving when  $\sigma = 0.050$ . This is because the phase oscillators almost stopped. This result suggests that the oscillator may have stopped at a stable equilibrium point except when the average phase difference  $\bar{\phi}$  did not converge to 0 rad. In other words, there was a stable equilibrium point that satisfies the following equation.

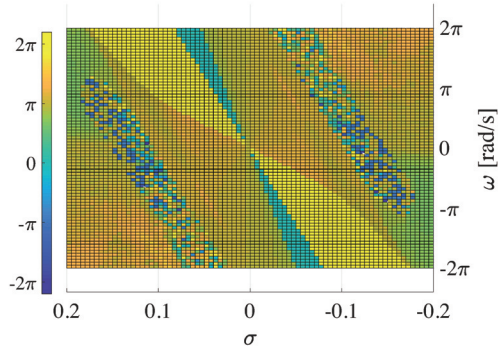
$$\omega \approx \sigma f_{mi} \cos \theta \quad \dots \dots \dots (9)$$

If the state of the pendulum satisfied the equation,  $\dot{\phi} \approx 0$ , the phase oscillator fell into a steady state.

**Figures 5, 7, and 9** indicate that cooperative relationships between the MPAs and some autonomous motions of the pendulum were generated by changing the tension feedback control law's parameters.



(a) Average phase difference with initial phase difference 0 rad ( $\sigma$ - $\omega$  plane)



(b) Average phase difference with initial phase difference  $\pi$  rad ( $\sigma$ - $\omega$  plane)

**Fig. 10.** The simulation results of tension feedback with initial phase difference 0 or  $\pi$  rad.

### 3.4. Analysis of the Effect of Initial Phase Difference

**Figure 10** shows the simulation result when the initial phase difference was changed from  $\pi/2$  rad. **Fig. 10(a)** shows the average phase difference  $\bar{\phi}$  with initial phase difference 0 rad. In this case, no change in phase difference occurs when the initial phase difference is 0 rad. The phase oscillators that determine the input pressures of MPAs show the same behavior since the phase difference is 0 rad.  $\theta$  and  $\dot{\theta}$  are equal to 0 when the pendulum stands still, therefore the MPA's length  $L_{mi}$  ( $i = 1, 2$ ) and contraction velocity  $v_i$  are equal between actuators because of Eqs. (3) and (4). Consequently, the MPA's tensions are equal because of Eq. (5). When the tensions are equal,  $\phi_1 = \phi_2$  because the angular velocities of two oscillators are equal. As a result, the phase difference does not change from 0 rad. From above,  $\phi = 0$  is one of the equilibrium points of the system.

**Figure 10(b)** shows the average phase difference  $\bar{\phi}$  with initial phase difference  $\pi$  rad. Comparing **Figs. 10(b)** and **6(a)**, the area of region where the average phase difference  $\bar{\phi}$  become 0 rad or  $2\pi$  rad with the initial phase difference  $\pi$  rad become smaller than that with the initial phase difference  $\pi/2$  rad. This is probably due to  $\phi = 0$  may be one of the locally stable equilibrium points of the system. If it were correct, there would be an attractor region neighborhood 0 rad or  $2\pi$  rad. Thereafter, once the

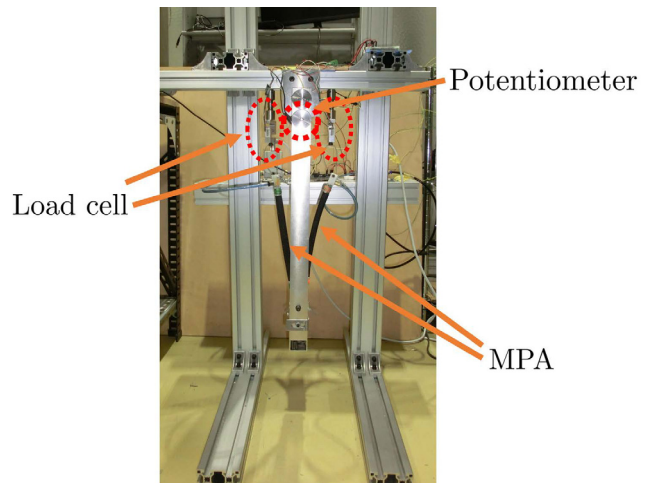


**Fig. 11.** Experimental setup of 1-DOF pendulum.

phase difference enters the region in the process of changing the phase difference due to the tension feedback, it will converge to 0 rad or  $2\pi$  rad. Therefore, it is considered that the area of the region where the average phase difference  $\bar{\phi}$  becomes 0 rad or  $2\pi$  rad with initial phase difference  $\pi/2$  rad is large because the initial phase difference  $\pi/2$  rad is closer to 0 rad or  $2\pi$  rad than the initial phase difference  $\pi$  rad. The stability of the equilibrium point  $\phi = 0$  can contribute to the realization of various resting postures. Besides, destabilizing the equilibrium point  $\phi = 0$  can promote the transition of the pendulum to another mode of motion. Therefore, a more detailed stability analysis of  $\phi = 0$  is significant and necessary.

When the average phase difference transitions, the average phase difference transitions to the around  $\bar{\phi} = 0$  or  $\bar{\phi} = \pi$ . Therefore, in this paper, the result of the initial phase difference  $\phi = \pi/2$  is focused because the change in the average phase difference is clear (**Fig. 6**). And the results of the initial phase difference  $\phi = 0$  and  $\pi$  are discussed for comparison with that of  $\phi = \pi/2$  (**Fig. 10**). The other results are likely to be interpolated into the results of  $0 \sim \pi/2 \sim \pi$ , but a detailed analysis of the effect of the initial phase difference is a subject for future study.

## 4. Verification of Cooperative Movement of MPAs with Experimental System

Next, we verified whether the proposed tension feedback control generated cooperation between the MPAs and if the cooperative relationship changed depending on the parameters on an experimental system.

### 4.1. 1-DOF Pendulum Machine

**Figure 11** shows the developed experimental system based on **Fig. 2(b)**. The pendulum was constructed by stacking two aluminum plates. A stainless-steel shaft was passed through the aluminum plates, and the pendulum can freely rotate around the shaft. The shaft was con-

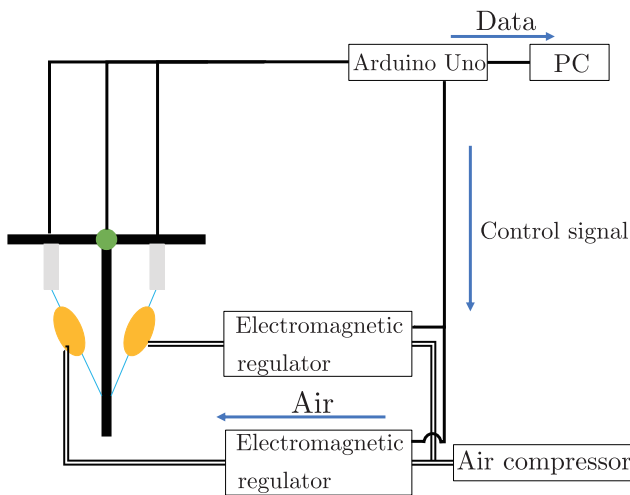


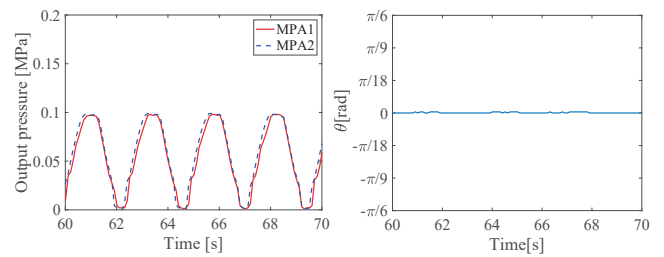
Fig. 12. Schematic of experimental setup.

nected to the base that supports the rod pendulum. Two antagonized MPAs were attached between the rod pendulum and the base, and the rod pendulum was driven by applying input pressure to the MPA. The ball joint (ASA Electronics Industry: MBD20-10-10) and the load cell (SNC: SC301A-100kg-V50) were connected to each MPA. The tension of the MPA can be measured using the load cell. The potentiometer (TOCOS: RA30Y20S B102) is attached to the pendulum, and the potentiometer is connected to the shaft via a gear. Therefore, the angle of the pendulum can be measured by the potentiometer.

The experimental environment around the actual machine is shown in Fig. 12. Compressed air was sent to each MPA via the electro-pneumatic regulator (SMC: ITV1050-212B). The electro-pneumatic regulator adjusted the pressure of air input. The microcomputer (Arduino: Arduino Uno) sends the value of the input pressure of MPAs, which is determined with Eqs. (6) and (7), to the regulators. The data of MPA's tension and the angle measured by the load cell and the potentiometer are sent to the microcomputer. The tension of MPAs, the pendulum angle, and the input to regulators are recorded on a PC via a microcomputer. In addition, the output value from regulators is also recorded to verify that compressed air was actually sent to MPAs.

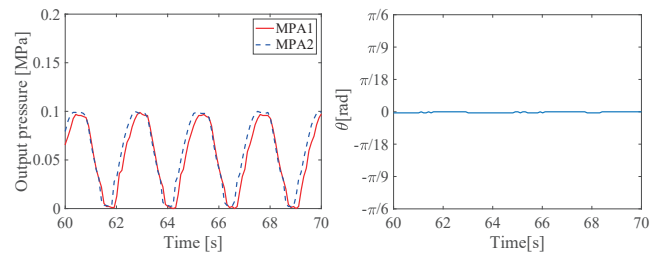
#### 4.2. Conditions of Verification Experiment

To investigate the cooperation between MPAs using the proposed tension feedback control, we compared the results of experiments under various conditions. In the first case, the initial phase difference  $\phi_0$  was set as 0 rad. Experiments were conducted for the positive (0.01) and negative ( $-0.01$ ) feedback gains  $\sigma$ . Furthermore, the pressure amplitude  $A$  was 0.05 MPa and the intrinsic angular velocity  $\omega$  was  $0.8\pi$  rad/s. In the second case, the initial phase difference was set to  $\pi/2$  rad. Similar to the first case, positive (0.01) and negative ( $-0.01$ ) feedback gains  $\sigma$  were used. In this case, the pressure amplitude was 0.075 MPa, and the intrinsic angular velocity was



(a) Input pressure of MPAs  $P'_i$  (b) Pendulum angle  $\theta$

Fig. 13. Experiment result with initial phase difference 0 rad and feedback gain  $\sigma = 0.01$ .



(a) Input pressure of MPAs  $P'_i$  (b) Pendulum angle  $\theta$

Fig. 14. Experiment result with initial phase difference 0 rad and feedback gain  $\sigma = -0.01$ .

$0.8\pi$  rad/s. For all the cases, the same parameters were used in the two-phase oscillators assigned to MPA1 and MPA2.

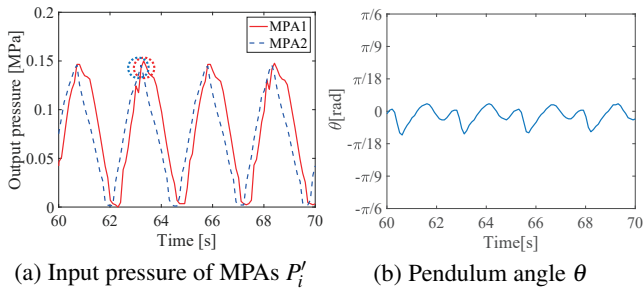
#### 4.3. Experimental Result with the Initial Phase Difference 0 rad

Figures 13 and 14 show the results while 60–70 s when the initial phase difference was 0 rad. Figs. 13 and 14 show the experimental results with positive feedback gain  $\sigma = 0.01$ , and that with negative feedback gain  $\sigma = -0.01$ . From Figs. 13(b) and 14(b), in both cases, the amplitude of the pendulum angle is almost 0 rad. Moreover, it can be verified that waveforms of the input pressures of MPAs are in good agreement, that is, the phase difference did not change from 0 rad despite the tension control law.

The reason for the behavior is as follows. When the initial phase difference is 0 rad, the input pressures of MPAs are equal, and the tensions of MPAs  $f_{m1}$ ,  $f_{m2}$  become equal. If  $f_{m1} = f_{m2}$ , the pendulum does not swing because the MPA tension is balanced. In such a situation, the two-phase oscillators move at the same velocity, according to Eq. (6). As a result, the phase difference remains unchanged. This result is consistent with Fig. 10(a).

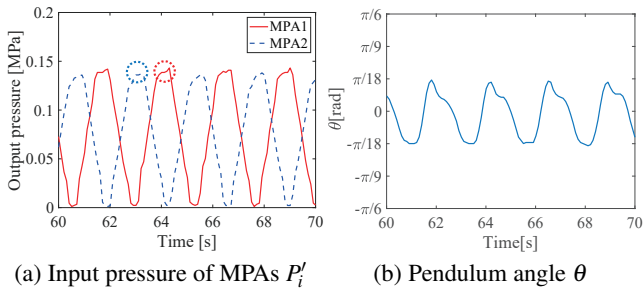
#### 4.4. Experimental Result with the Initial Phase Difference $\pi/2$ rad

Figures 15 and 16 shows the experimental results with the initial phase difference was  $\pi/2$  rad. When the feedback gain was  $\sigma = 0.01$ , the input pressures of MPAs were slightly shifted, as shown in Fig. 15(a). This indicates that the phase difference transitioned from  $\pi/2$  rad



(a) Input pressure of MPAs  $P'_i$  (b) Pendulum angle  $\theta$

**Fig. 15.** Experiment result with initial phase difference  $\pi/2$  rad and feedback gain  $\sigma = 0.01$ .



(a) Input pressure of MPAs  $P'_i$  (b) Pendulum angle  $\theta$

**Fig. 16.** Experiment result with initial phase difference  $\pi/2$  rad and feedback gain  $\sigma = -0.01$ .

in a decreasing direction. Consequently, as shown in **Fig. 15(b)**, the amplitude of the pendulum also remained small because the phase difference remained small. The reason for the behavior is that if the feedback gain was positive, the velocity of the phase oscillator decreased when the MPA tension was generated by the tension feedback control. This increased the time during which the MPA tension was generated. As a result, the phase difference changed such that the MPA antagonized and a larger tension was obtained. Here, the results with the parameters used in this experiment correspond to the region ii of **Figs. 6(b)** and **9** in the numerical simulation. As in the simulation results, the phase oscillator was not stopped in the experiment. However, the result that the phase difference transitioned in the direction of decreasing became consistent.

**Figure 16** shows the results with negative feedback gain. From **Fig. 16(a)**, it can be seen that two MPAs alternately contracted and expanded, and the phase difference transitioned from  $\pi/2$  rad in the increasing direction with negative feedback gain. As a result, the pendulum also realized stable periodic motion, as shown in **Fig. 16(b)**. If the feedback gain was negative, the velocity of the phase oscillator increased when MPA tension was generated by the tension feedback control. This changed the phase difference so that the MPA tensions did not antagonize and avoid the generation of large tensions. As a result, the phase difference transitioned from  $\pi/2$  rad in an increasing direction. This result corresponds to oscillation mode of the region III<sub>a</sub> in **Fig. 6(a)**. The difference in the magnitude of the intrinsic angular velocity and feedback gain between **Fig. 5** in the numerical simulation and **Fig. 16** in the experiments was due to modeling errors and vari-

ous error factors that exist in the actual machine such as tension model and attachment method of MPA.

Based on these experiments, it could be verified that the antagonized MPAs can autonomously change the relationship and realize a cooperative movement by implementing the tension feedback in an experimental system. These results suggested that by selecting the feedback gain appropriately for the intrinsic angular velocity, the desired MPA cooperative relationship can be generated, and various movements can be realized. To realize the movements, it is necessary to clarify the mechanism by which these movements are generated. Theoretical analysis of the system with the proposed tension feedback is for future study.

## 5. Conclusion

The purpose of this study was to realize the cooperation between antagonized MPAs by applying tension feedback control to the musculoskeletal model. In this study, we analyzed the 1-DOF pendulum motion with MPA antagonistically arranged as the simplest musculoskeletal model. As a control law for generating the cooperation of MPAs, we proposed tension feedback control. Through numerical simulations, it was verified that the relationship between MPAs changed depending on parameters such as the intrinsic angular velocity and the feedback gain. As a result, the pendulum exhibited various motions, and the tension control law generated some oscillation modes of the pendulum. We further developed the experimental system and conducted verification experiments by implementing the tension feedback control law to MPAs. Similar to the numerical simulations, it was also verified that MPAs realized various cooperative relationships. Thereafter, the pendulum exhibited various movements on the actual machine. Based on these results, according to the parameters in the robot and the control law, an autonomous cooperative relationship between the MPAs could be generated by using the proposed tension feedback control. Further studies are required to consider the cause of the cooperation between actuators.

The simulation results show that various oscillation modes were generated according to the parameters, and the change of the oscillation modes with the parameter changes was abrupt. This result suggests that the bifurcation phenomenon occurred in the system targeted in this study. Although the case of relatively slow transitions is examined in this paper, the parameters that cause immediate transitions are also confirmed in simulations. Theoretical analysis as nonlinear dynamical tension feedback of MPA for the investigation of the autonomous cooperative relationship generation mechanism is a future topic. It is also important to analyze the effects of initial phase difference and responsiveness in more detail and to discuss how the various modes are connected to achieve a variety of continuous robot motions.

**Acknowledgements**

This work was supported by JSPS KAKENHI Grant Numbers JP17H06150, JP19H04193, JP18K13718 and CREST, JST. We would like to thank Editage (www.editage.com) for English language editing.

**References:**

- [1] H. Kobayashi, T. Matsushita, Y. Ishida, and K. Kikuchi, "New robot technology concept applicable to human physical support The concept and possibility of the muscle suit (wearable muscular support apparatus)," *J. Robot. Mechatron.*, Vol.14, No.1, pp. 46-53, doi: 10.20965/jrm.2002.p0046, 2002.
- [2] K. Hosoda, Y. Sakaguchi, H. Takayama, and T. Takuma, "Pneumatic-driven jumping robot with anthropomorphic muscular skeleton structure," *Auton. Robots*, Vol.28, No.3, pp. 307-316, doi: 10.1007/s10514-009-9171-6, April 2010.
- [3] K. Nakada, T. Asai, and Y. Amemiya, "Biologically-inspired locomotion controller for a quadruped walking robot: Analog IC implementation of a CPG-based controller," *J. Robot. Mechatron.*, Vol.16, No.4, pp. 397-403, doi: 10.20965/jrm.2004.p0397, 2004.
- [4] G. Taga, Y. Yamaguchi, and H. Shimizu, "Self-organized control of bipedal locomotion by neural oscillators in unpredictable environment," *Biol. Cybern.*, Vol.65, No.3, pp. 147-159, doi: 10.1007/BF00198086, July 1991.
- [5] G. Liu, M. Habib, K. Watanabe, and K. Izumi, "The design of central pattern generators based on the Matsuoka oscillator to generate rhythmic human-like movement for biped robots," *J. Adv. Comput. Intell. Inform.*, Vol.11, No.8, pp. 946-955, 2007.
- [6] Y. Fukuoka, H. Katabuchi, and H. Kimura, "Dynamic locomotion of quadrupeds Tekken3&4 using simple navigation," *J. Robot. Mechatron.*, Vol.22, No.1, pp. 36-42, doi: 10.20965/jrm.2010.p0036, 2010.
- [7] D. Owaki, T. Kano, K. Nagasawa, A. Tero, and A. Ishiguro, "Simple robot suggests physical interlimb communication is essential for quadruped walking," *J. R. Soc. Interface*, Vol.10, No.78, pp. 1-11, doi: 10.1098/rsif.2012.0669, 2013.
- [8] M. A. Gorassini, A. Prochazka, G. W. Hiebert, and M. J. A. Gauthier, "Corrective responses to loss of ground support during walking. I. Intact cats," *J. Neurophysiology*, Vol.71, pp. 603-610, doi: 10.1152/jn.1994.71.2.603, 1994.
- [9] G. W. Hiebert, M. A. Gorassini, W. Jiang, A. Prochazka, and K. G. Pearson, "Corrective responses to loss of ground support during walking. II. Comparison of intact and chronic spinal cats," *J. Neurophysiology*, Vol.71, pp. 611-622, doi: 10.1152/jn.1994.71.2.611, 1994.
- [10] N. Tsagarakis, "Improved modeling and assessment of pneumatic muscle actuators," *Proc. IEEE Conf. on Robotics and Automation*, San Francisco, CA, pp. 3641-3646, doi: 10.1109/ROBOT.2000.845299, 2000.
- [11] B. Tondu and P. Lopez, "Modeling and control of McKibben artificial muscle robot actuators," *IEEE Contr. Syst. Mag.*, pp. 15-38, doi: 10.1109/37.833638, April 2000.
- [12] S. Yoshida, D. Nakanishi, K. Naniwa, Y. Sugimoto, and K. Osuka, "Verification of linear approximation model of McKibben pneumatic actuator," *Trans. of the JSME*, Vol.85, No.878, pp. 1-13, doi: 10.1299/transjsme.18-00498, 2019 (in Japanese).
- [13] Y. Sugimoto, K. Naniwa, K. Osuka, and Y. Sankai, "Static and dynamic properties of McKibben pneumatic actuator for self-stability of legged-robot motion," *Adv. Robotics*, Vol.27, No.6, pp. 469-480, doi: 10.1080/01691864.2013.763007, 2013.
- [14] P. Meier, M. Lang, and S. Oberthur, "Reiterated tension testing of silicone elastomer," *Plastics, Rubber and Composites Macromolecular Engineering*, Vol.34, No.372-377, doi: 10.1179/174328905X59737, 2005.
- [15] D. Nakanishi, Y. Sugimoto, H. Honda, and K. Osuka, "Measurement experiments and analysis for modeling of McKibben pneumatic actuator," *J. Robot. Mechatron.*, Vol.28, No.6, pp. 830-836, doi: 10.20965/jrm.2016.p0830, 2016.

**Appendix A. Linear Approximation Model [12]**

The linear approximation model is based on the conservation law model proposed in our previous study, which was derived using the law of conservation of energy [13].

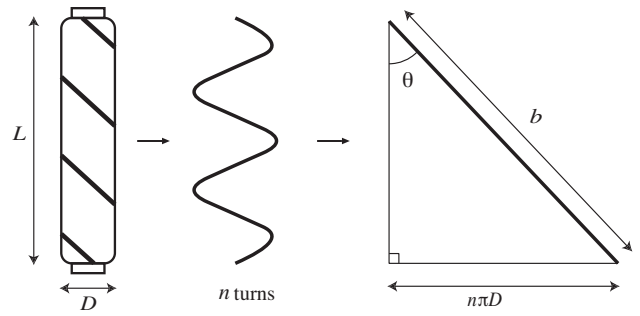


**Fig. 17.** The geometry of the actuator and the relationship between  $L$ ,  $D$ ,  $b$ , and  $n$  illustrated by the triangle [13].

The conservation law model is expressed as follows:

$$f_m(P', L, v) = -P' \frac{dV_b}{dL} + V_r \frac{dW}{dL} + \gamma v \dots \quad (10)$$

where  $L$  is the length of MPA,  $v$  is the contraction velocity of MPA,  $P'$  is the pressure of the MPAs,  $V_b$  is the air bag's volume,  $V_r$  is the volume of the rubber, and  $W$  is the strain energy density determined using the Mooney-Rivlin model, which is one of the super elastic models. The third term represents the dynamic characteristics of the MPA  $f_v$ . Sugimoto et al. found that  $f_v$  has a linear relationship with the contraction speed. Therefore,  $f_v = \gamma v$ , where  $\gamma$  is a constant, in the model.

Equation (10) is rewritten in detail as follows:

$$f_m(P', L, v) = -P' \frac{b^2 - 3L^2}{4\pi n^2} + V_r \left[ C_1 \left\{ \frac{2L}{L_0^2} - \frac{2L}{D_0^2 n^2 \pi^2} - \frac{2L_0^2 D_0^2 n^2 \pi^2 (b^2 - 2L^2)}{L^3 (b^2 - L^2)^2} \right\} + C_2 \left\{ -\frac{2L_0^2}{L^3} + \frac{2D_0^2 n^2 \pi^2 L}{(b^2 - L^2)^2} + \frac{2Lb^2 - 4L^3}{L_0^2 D_0^2 n^2 \pi^2} \right\} \right] + \gamma v. \quad (11)$$

**Fig. 17** presents the parameters used in the model. These parameters are constants. The subscript 0 in Eq. (11) indicates the initial value. The Mooney-Rivlin constants  $C_1, C_2$  refers to the value in the previous research [14]. The details of this model are given in [13].

On the contrary, Nakanishi et al. discussed the effects of MPA length and pressure on dynamic properties [15]. As a result, it was shown that the relationship between the MPA's tension  $f_m$ , the contraction velocity  $v$ , and the MPA's length  $L$  could be described by a plane in three-dimensional space. Based on the result, the linear sum model of the MPA tension model is proposed as follows:

$$f_m = b_0 + b_1 v + b_2 L. \dots \dots \dots (12)$$

The coefficients ( $b_0, b_1, b_2$ ) are in a linear relationship with the air pressure  $P'$ . Therefore, Eq. (12) is rewritten in detail using the intercepts ( $q_0, r_0, s_0$ ) and the slopes ( $q_1, r_1, s_1$ ) as follows:

$$f_m = (q_0 + q_1 P') + (r_0 + r_1 P') v + (s_0 + s_1 P') L = q_1 P' + s_1 P' L + s_0 L + q_0 + (r_0 + r_1 P') v. \quad (13)$$

The expression for the linear sum model is simpler than that of the conservation law model. However, the parameters in the linear sum model need to be identified every time the MPA conditions are altered. The details of this model are given in [15].

From the abovementioned two models, Yoshida et al. rewrote Eq. (10) at first as follows:

$$f_m = -P'G_1(L) + G_2(L) + \gamma v, \dots \dots \dots (14)$$

where  $G_1$  and  $G_2$  are the functions of the MPA's length defined as follows:

$$G_1(L) = \frac{b^2 - 3L^2}{4\pi n^2}, \dots \dots \dots (15)$$

$$G_2(L) = V_r \left[ C_1 \left\{ \frac{2L}{L_0^2} - \frac{2L}{D_0^2 n^2 \pi^2} - \frac{2L_0^2 D_0^2 n^2 \pi^2 (b^2 - 2L^2)}{L^3 (b^2 - L^2)^2} \right\} + C_2 \left\{ -\frac{2L_0^2}{L^3} + \frac{2D_0^2 n^2 \pi^2 L}{(b^2 - L^2)^2} + \frac{2Lb^2 - 4L^3}{L_0^2 D_0^2 n^2 \pi^2} \right\} \right]. (16)$$

By Taylor expansion around  $\tilde{L}$ , which is a certain MPA's length, Eq. (14) can be linearly approximated as follows:

$$f_m = f_m(\tilde{L}, P') + \left( -\frac{dG_2(\tilde{L})}{dL} \tilde{L} + P' \tilde{L} \frac{dG_1(\tilde{L})}{dL} G_1(L) \right) + \gamma v + \left( \frac{dG_2(\tilde{L})}{dL} - P' \frac{dG_1(\tilde{L})}{dL} \right) L = c_0 + c_1 v + c_2 L (17)$$

Eq. (17) has a similar expression with the linear sum model (Eq. (12)), and the coefficients in Eq. (17) are linearly related to  $P'$ . Furthermore, Eq. (17) is rewritten as follows:

$$f_m = \left( -G_1(\tilde{L}) + \tilde{L} \frac{dG_1(\tilde{L})}{dL} \right) P' + \left( \frac{dG_1(\tilde{L})}{dL} \right) P' L + \left( \frac{dG_2(\tilde{L})}{dL} \right) L + \left( G_2(\tilde{L}) - \frac{dG_2(\tilde{L})}{dL} \tilde{L} \right) L + \gamma v = S_1 P' + S_2 P' L + S_3 L + S_4 + \gamma v (S_{1,2,3,4} = \text{const.}) \dots \dots \dots (18)$$

This model is the linear approximation model. Eq. (18) has the same expansion of variables and constants as Eq. (13). However, coefficients in Eq. (18) are determined by the geometric structure of MPA and Mooney-Rivlin constant unlike the linear sum model. Additional details can be found in [12]. Although  $\tilde{L}$  is defined as the midpoint between the maximum length  $L_{\max} = L_0$  and the geometric minimum length  $L_{\min} = L_0/\sqrt{3}$  in [12], we define  $\tilde{L}$  as the natural length of MPA in this paper because the displacement of the MPA's length oscillated around its natural length.



**Name:**  
Takahiro Goto

**Affiliation:**  
Master Student, Department of Mechanical Engineering, Osaka University

**Address:**  
2-1 Yamadaoka, Suita, Osaka 565-0871, Japan

**Brief Biographical History:**  
2019- Master Student, Osaka University

**Membership in Academic Societies:**  
• The Japan Society of Mechanical Engineers (JSME)



**Name:**  
Yasuhiro Sugimoto

**Affiliation:**  
Associate Professor, Department of Mechanical Engineering, Osaka University

**Address:**  
2-1 Yamadaoka, Suita, Osaka 565-0871, Japan

**Brief Biographical History:**  
2005- Research Associate, Kyoto University  
2009- Assistant Professor, Osaka University  
2014- Associate Professor, Osaka University

**Main Works:**  
• Y. Sugimoto, T. Kibayashi, M. Ishikawa, and K. Osuka, "Nonlinear Control by Coupled Oscillator: from Nonholonomic Systems to Quasi-Passive Dynamic Walker," Nonlinear Theory and Its Applications, Vol.E6-N, No.4, pp. 475-487, 2015.

**Membership in Academic Societies:**  
• The Japan Society of Mechanical Engineers (JSME)  
• The Robotics Society of Japan (RSJ)  
• The Society of Instrument and Control Engineers (SICE)



**Name:**  
Daisuke Nakanishi

**Affiliation:**  
Assistant Professor, Department of Control Engineering, National Institute of Technology, Matsue College

**Address:**  
14-4 Nishi-ikuma, Matsue, Shimane 690-8518, Japan

**Brief Biographical History:**  
2014- Research Fellow (DC1), Japan Society for the Promotion of Science  
2017- Assistant Professor, National Institute of Technology, Matsue College

**Main Works:**  
• D. Nakanishi, Y. Sueoka, Y. Sugimoto, and K. Osuka, "Numerical analysis and experimental verification for standing posture and joint stiffness of a 2-dimensional legged robot driven by McKibben pneumatic actuator," *Trans. of SICE*, Vol.51, No.12, pp. 858-865, 2015.

**Membership in Academic Societies:**  
• The Japan Society of Mechanical Engineers (JSME)  
• The Institute of Systems Control and Information Engineers (ISCIE)

---



**Name:**  
Keisuke Naniwa

**Affiliation:**  
Academic Researcher, Research Center of Mathematics for Social Creativity, Research Institute for Electronic Science, Hokkaido University

**Address:**  
Kita 12, Nishi 7, Kita-ku, Sapporo, Hokkaido 060-0812, Japan

**Brief Biographical History:**  
2011- Omron Corp.  
2014- Doctoral Student, Graduate School of Engineering, Osaka University  
2017- Research Institute for Electronic Science, Hokkaido University

**Main Works:**  
• "Defecation initiates walking in the cricket *Gryllus bimaculatus*," *J. of Insect Physiology*, Vol.112, pp. 117-122, Jan. 2019.

**Membership in Academic Societies:**  
• The Zoological Society of Japan (ZSJ)  
• The Robotics Society of Japan (RSJ)

---



**Name:**  
Koichi Osuka

**Affiliation:**  
Professor, Department of Mechanical Engineering, Osaka University

**Address:**  
2-1 Yamadaoka, Suita, Osaka 565-0871, Japan

**Brief Biographical History:**  
1986- Research Associate / Assistant Professor, Osaka Prefecture University  
1998- Assistant Professor, Kyoto University  
2003- Professor, Kobe University  
2009- Professor, Osaka University

**Main Works:**  
• Y. Sueoka, Y. Sato, M. Ishitani, and K. Osuka, "Analysis of push-forward model for swarm-like collective motions," *Artificial Life and Robotics*, Vol.24, No.4, pp. 460-470, 2019.  
• Y. Sueoka, T. Tahara, M. Ishikawa, and K. Osuka, "Statistical Exploration of Distributed Pattern Formation Based on Minimalistic Approach," *J. Robot. Mechatron.*, Vol.31, No.6, pp. 905-912, 2019.  
• K. Mak, K. Osuka, Y. Sugimoto, and T. Wada, "MACROTIS: a cubic robot with snap-through buckling mechanisms for achieving high freedom of movement," *J. Robot. Mechatron.*, Vol.31, No.3, pp. 500-506, 2019.

**Membership in Academic Societies:**  
• The Philosophical Association of Japan (PAJ)  
• The Japan Society of Mechanical Engineers (JSME)  
• The Robotics Society of Japan (RSJ)

---